



**HAL**  
open science

## **Influence of Electronic Irradiation on Failure and Hardness Properties of Pure Silica Glasses**

M. Barlet, J-M. Delaye, M. Gennisson, R. Caraballo, B. Boizot, Daniel Bonamy, C.L. Rountree

► **To cite this version:**

M. Barlet, J-M. Delaye, M. Gennisson, R. Caraballo, B. Boizot, et al.. Influence of Electronic Irradiation on Failure and Hardness Properties of Pure Silica Glasses. 2nd International Summer School on Nuclear Glass Wasteform: Structure, Properties and Long-Term Behavior, SumGLASS 2013, Sep 2013, Pont du Gard, France. pp.286-293, 10.1016/j.mspro.2014.10.037 . cea-01120966

**HAL Id: cea-01120966**

**<https://cea.hal.science/cea-01120966>**

Submitted on 27 Feb 2015

**HAL** is a multi-disciplinary open access archive for the deposit and dissemination of scientific research documents, whether they are published or not. The documents may come from teaching and research institutions in France or abroad, or from public or private research centers.

L'archive ouverte pluridisciplinaire **HAL**, est destinée au dépôt et à la diffusion de documents scientifiques de niveau recherche, publiés ou non, émanant des établissements d'enseignement et de recherche français ou étrangers, des laboratoires publics ou privés.



2nd International Summer School on Nuclear Glass Wasteform: Structure, Properties and Long-Term Behavior, SumGLASS 2013

## Influence of electronic irradiation on failure and hardness properties of pure silica glasses

M. Barlet<sup>a</sup>, J.-M. Delaye<sup>b</sup>, M. Gennisson<sup>b</sup>, R. Caraballo<sup>b</sup>, B. Boizot<sup>c</sup>, D. Bonamy<sup>a</sup>, C. L. Rountree<sup>a,\*</sup>

<sup>a</sup>CEA, IRAMIS, SPEC, SPHYNX, Grp. Complex Systems and fracture, F-91191 Gif-sur-Yvette, France

<sup>b</sup>CEA, DEN, DTCD, SECM, LMPA, CEA Marcoule, BP17171 30207 Bagnols-sur-Cèze, France

<sup>c</sup>Laboratoire des Solides Irradiés, UMR 7642 CEA-CNRS-Ecole Polytechnique, 91128 Palaiseau, France

### Abstract

This paper's focus is the failure and hardness properties of pure amorphous silica (Corning 7980®) after  $\beta$ -irradiation at different doses (0-2 GGy). Crack propagation takes place in the SCC regime ( $10^{-7}$ - $10^{-10}$  m.s<sup>-1</sup>) and Vickers indentation techniques probe the hardness properties of the samples. Irradiation is found to create point defects which mainly include E' centers, Non-Bridging Oxygen Hole Centers and Peroxy Radicals.  $\beta$ -irradiation herein invokes minor changes in the structure. A small effect of  $\beta$ -irradiation on SCC and hardness variations cannot be eliminated, despite minute variations in the SCC and the hardness properties.

© 2014 The Authors. Published by Elsevier Ltd. This is an open access article under the CC BY-NC-ND license

(<http://creativecommons.org/licenses/by-nc-nd/3.0/>).

Selection and peer-review under responsibility of the scientific committee of SumGLASS 2013

**Keywords:** Silica glass, Electronic irradiation, Microstructure, Mechanical properties

### 1. Introduction

The brittleness of glass is the most limiting factor in its widespread applications. With a multitude of research dedicated to this material (Wiederhorn (1967); Wiederhorn and Bolz (1970); Rountree et al. (2002); Wiederhorn et al. (2007a,b); Kalia et al. (2003); Celarie et al. (2003, 2007); Lechenault et al. (2010, 2011); Ciccotti (2009)), it's commonly understood that water molecules play a fundamental role in stress corrosion crack propagation in glasses (Wiederhorn (1967); Wiederhorn and Bolz (1970)). Yet the mechanisms at the crack tip which lead to the failure of glass are not fully understood (Wiederhorn et al. (2007a); Ciccotti (2009)). Stress enhancement at the crack tip makes the fracture behavior drastically sensitive to the presence of microstructure inhomogeneities down to very small scales. This makes it difficult to anticipate how structural alterations would affect the failure properties at the continuum-level scale. This question is of uttermost importance to assess the durability of glass components under irradiation. Extensive studies on the generation of point defects and structural variations of silica glasses under  $\beta$ -irradiation exist in literature (Boizot et al. (2003); Agnello et al. (2002); Weeks (1956)). In contrast, the effects of  $\beta$ -irradiation on the fracture properties (and especially stress corrosion cracking, SCC, properties) remain widely unknown.

\*Corresponding author. Tel.: +33-169-082-655; fax:+33-169-082-446.

E-mail address: [cindy.rountree@cea.fr](mailto:cindy.rountree@cea.fr) (C. L. Rountree)

The study herein concentrates on the failure of pure amorphous silica.  $\text{SiO}_2$  is frequently one of the glass formers in glassy systems involving (external or self-generated) irradiation (satellites, glass packages of radioactive waste...). Irradiation gradually alters the atomic arrangement at the microstructure level. An open question is how these variations modify the failure and hardness properties of glasses.  $\alpha\text{-SiO}_2$  samples were irradiated by means of a Van de Graaff electron accelerator with integrated doses of up to 2 GGy with energetic electrons (2.5 MeV, 13  $\mu\text{A}$ ). The induced structural alterations are probed by means of Electron Paramagnetic Resonance (EPR) and Raman spectroscopies reveal the creation of paramagnetic defects, quantify their amount, and point out possible structural variations. The impact of irradiation on the hardness and SCC failure properties are finally monitored. These results provide keys to understand how electron irradiation impacts the failure mechanism and the hardness properties.

## 2. Experimental

Pure amorphous silica samples are Corning 7980<sup>®</sup> of which the composition is certified to 99.9% pure silica. Experiments herein do not depend on the sample geometry with the exception of the stress corrosion cracking (SCC) experiments. SCC experiments require DCDC (Double Cleavage Drilled Compression) samples (Janssen (1974)). The geometry of the samples are cuboids of size  $0.8 \times 2 \times 25 \text{ mm}^3$  with a 0.4 mm diameter hole drilled in the center. The sample thickness, 0.8 mm, insures homogeneous irradiation. Thus all experiments employ DCDC sample geometry.

*Electronic irradiation conditions.* The sample irradiation employs a Van de Graaff accelerator (SIRIUS) at LSI (Ecole Polytechnique, Palaiseau, France). SIRIUS bombards samples with 2.5 MeV electrons with an average current of 13  $\mu\text{A}$  to prevent significant heating of the sample. Moreover, the sample temperature remains below 40°C to avoid recombination of defects. The integral doses for samples herein are 1 and 2 GGy.

*Electron paramagnetic resonance (EPR).* Electron paramagnetic resonance (EPR) spectroscopy reveals point defects ( $\text{E}'$ , NBOHC, Peroxy radical,...) arising during  $\beta$ -irradiation. EPR tests herein employ LSI's MX Bruker EPR spectrometer. This equipment has a 100 kHz field modulation. Experiments utilize microwave powers of 10  $\mu\text{W}$ , 1 mW and 10 W. The measurements take place in ambient conditions and use a fixed frequency (X band  $\nu=9.82 \text{ GHz}$ ).

*Raman analysis.* Raman analysis employs a JobinYvon HR800 spectrometer. The laser is a YAG laser ( $\lambda=532 \text{ nm}$ ) with an adjustable output power. Maintaining a low laser power prevents significant heating of the samples. Resulting spectra are the average of ten measurements accumulated over ten seconds.

*Vickers microindentation tests.* Invoking Vickers microindentation test provides an estimate of the material's hardness plus the amount of densification. The indentation load,  $F$ , is 50 g maintained for 15 s at the maximum load. Examining the resulting imprints gives 4 parameters:

1. Indentation depth:  $d_i$
2. Indentation diagonal length:  $l_i$
3. Indentation volume:  $V_i^-$ , volume measured below the free surface
4. Volume of pileup:  $V_i^+$ , volume measured above the free surface

Knowing  $F$  and  $l_i$ , the Vickers hardness ( $H_V$ ) is as follows:

$$H_V = \frac{1.8544F}{l_i^2} \quad (1)$$

Under the indenter, glasses can densify (Arora et al. (1979); Ernsberg (1968); Perriot et al. (2011, 2006)) and an indentation impression can be partially recovered by thermal annealing (Neely and Mackenzie (1968); Bridgman and Simon (1953)). Yoshida et. al. (2001,2005) propose a 3-dimensional technique to characterize the indentation imprints before and after annealing and subsequently estimate the fraction of densification. After indentation and imaging, samples undergo a 2 h annealing treatment at  $0.9 T_g$  in air. A null viscous flow assumption can be made here since Maxwell's relaxation time is significantly greater than the annealing time. On the other hand, the annealing time is sufficiently long to achieve the complete recovery of the densified regions (Mackenzie (1963b); Yoshida et al. (2001, 2005); Hetherington (1964)).

The imprint topography are imaged prior and after annealing by means of an atomic force microscope (Dimension Icon Nanoscope V Bruker). The image acquisition mode is the PeakForce Tapping. The AFM cantilever (Bruker's RTESPA) is a silicon tip with a nominal radius of 8 nm and a nominal cantilever force constant of 40 N/m. The scan size is sufficiently large with respect to the imprint size to allow correcting the AFM image planarity. Typically the image sizes are greater than twice the indentation diagonal. In-plane and out-of-plane AFM measurements have less than 2% error (i.e. the X and Y directions) and about 2% (i.e. Z direction), respectively. Processing the AFM images gives  $d_i$ ,  $l_i$ ,  $V_i^-$  and  $V_i^+$  (figure 1) prior to annealing. After annealing the indent imprints is observed to change in shape, which is linked to the recovery of densified areas under the indenter Neely and Mackenzie (1968); Bridgman and Simon (1953); Yoshida et al. (2005, 2007). A second image processing gives  $d_a$ ,  $l_a$ ,  $V_a^-$  and  $V_a^+$  (figure 1) after annealing. Annealing and post-treatment of the AFM images gives the recovery volume ratio,  $V_R$ , (Yoshida et al. (2005)):

$$V_R = \frac{(V_i^- - V_a^-) + (V_a^+ - V_i^+)}{V_i^-} \quad (2)$$

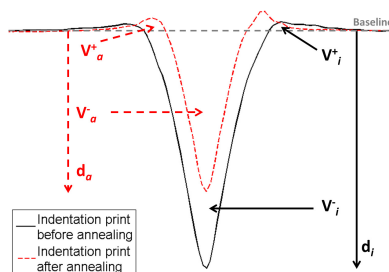


Fig. 1. Example of the variation in the indentation prints before and after annealing

**Fracture experiments.** Fracture experiments employ Double Cleavage Drilled Compression (DCDC) samples (Janssen (1974)) well adapted to study the fracture behavior of glass under stress corrosion. Samples undergo a compressive load applied normal to the  $0.8 \times 2 \text{ mm}^2$  surfaces via a Deben machine. Due to the overall geometry of the sample (He et al. (1995); Pallares et al. (2009)), the crack front propagates in mode I (opening mode). This gradual increase is obtained by bringing closer the two jaws of the Deben loading machine at a constant rate ( $0.02 \text{ mm} \cdot \text{min}^{-1}$ ) (Bonamy et al. (2006); Rountree et al. (2007, 2010)). Once the two precracks are initiated, the jaws displacement is stopped, and the precracks relax. Subsequently, the stress on the glass sample is set and held fixed for a period of time. A stationary tubular microscope attached to an IDS uEye (1465LE-C) camera images the crack propagation at the specimen surface. The Deben machine sits on three Newport linear stage motors (LTA motor for focusing options and two CMA motors to follow the crack front). These motors permit the sample to be displaced when the crack front moves outside the tubular microscope's zone of observation. Image processing provides the time-evolution of the crack tip, and the crack velocity is subsequently inferred. The Deben loading machine monitors the force applied to the samples. From this, the stress intensity factor,  $K_I$ , is calculated using the formulas provided in (He et al. (1995); Pallares et al. (2009)). The fracture experiments are enclosed in a glove box, which controls temperature and humidity. For pristine samples and 2 Ggy irradiated samples, three and two samples were broken, respectively. Error bars in  $v$  vs  $K_I$  curves correspond to the standard deviation of these measurements. For 1.5 Ggy samples, one sample was broken. Error bars in  $v$  vs  $K_I$  curves correspond to the standard deviation of pristine samples.

### 3. Results

#### 3.1. Structural results

EPR spectra reveal the creation of paramagnetic defects in a-SiO<sub>2</sub> due to  $\beta$ -irradiation (figure 2 left). A null EPR signal occurs for non-irradiated silica glass, and a non-zero signal in the irradiated samples. Literature (Weeks (1956);

Griscom (2011)) permits the interpretation of the signals. The weak signal around  $g \sim 2.002$  is well known as the  $E'$  center and evidences as an electron trapped at an oxygen vacancy ( $\equiv Si^{\cdot}$ ) (Weeks (1956)). A broad signal exists around  $g \sim 2.004 - 2.008$  which is attributed to Non-Bridging Oxygen Hole Centers ( $\equiv Si - O^{\cdot}$ ) or Peroxy Radical defects ( $\equiv Si - O - O^{\cdot}$ ). For the doses herein, the total amount of defects increases with the irradiation dose (figure 2 right).

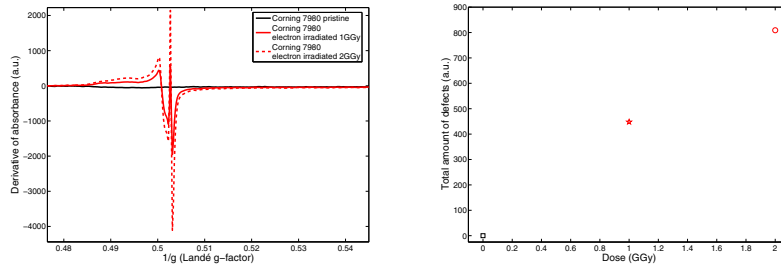


Fig. 2. (Left) EPR spectra of Corning 7980® pristine and electron irradiated at 1 and 2 GGy ( $P=10$  mW,  $f=9.82$  GHz). (Right) Total amount of defects created in  $a\text{-SiO}_2$  at different integrated doses .

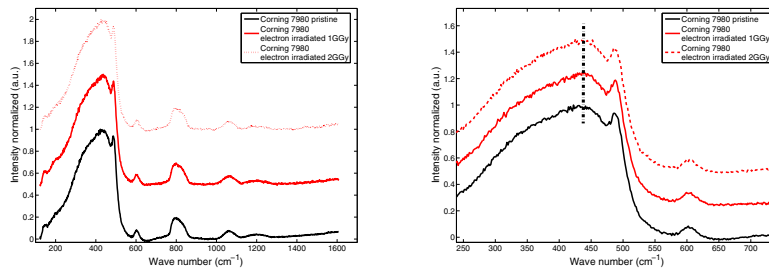


Fig. 3. (Left) Raman spectra normalized at the highest peak of pristine and electron irradiated samples at 1 and 2 GGy ( $\lambda=532$  nm). (Right) Raman spectra normalized and zoomed ( $250\text{-}700\text{cm}^{-1}$ ) in on the highest peak for pristine and 1 and 2 GGy electron irradiated samples ( $\lambda=532$  nm).

Figure 3 presents the Raman spectra for pristine and  $\beta$  irradiated samples (1 and 2 GGy) between  $150$  and  $1650\text{ cm}^{-1}$ . The black line represents the non-irradiated sample. The intense broad band around  $450\text{ cm}^{-1}$  dominates the Raman spectrum. Generally this broad peak corresponds to the bond bending vibrations of  $Si - O - Si$  angle which corresponds to the five- and six- membered ring structures. The sharp bands at  $490\text{ cm}^{-1}$  (D1) (respectively  $602\text{ cm}^{-1}$  (D2)) correspond to the symmetric oxygen breathing vibration of four (three membered) siloxane rings of  $SiO_4$  tetrahedra. The band at  $800\text{ cm}^{-1}$  reflexes the  $Si - O$  symmetric bond stretching. Weak Raman bands at  $1060\text{ cm}^{-1}$  and  $1200\text{ cm}^{-1}$  are attributed to asymmetric  $Si - O$  stretching vibration. No significant differences are observed in the Raman spectra between pristine and irradiated samples.

### 3.2. Mechanical properties

Mechanisms at the crack tip govern the failure behavior. Thus due to high stresses at the crack tip, minute defects can play a major role in SCC. Figure 4 presents the variations of the failure properties in the stress corrosion regime and the hardness for systems subjected to electron irradiation. It is well documented that the crack propagation velocity ( $v$ ) increases with the stress intensity factor ( $K_I$ ) (Wiederhorn (1967); Wiederhorn and Bolz (1970)):

$$v(K_I) = v_0 e^{\frac{bK_I - E^*}{RT}} \quad (3)$$

where  $E^*$  (activation energy at zero load) and  $b$  are fitting parameters which capture the effect of glass composition. The parameter  $v_0$  also depends on the partial pressure of the water vapor in the atmosphere (normally assumed to

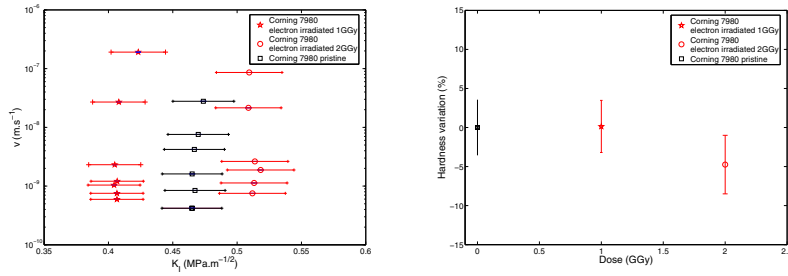


Fig. 4. (Left) Velocity of the crack front versus toughness ( $K_I$ ) in pristine and electron irradiated Corning 7980 samples at 1 and 2 GGy. Fracture experiments are conducted at  $T=27^\circ\text{C}$  and  $H=40\%$ . (Right) Hardness variation for pristine and electron irradiated (1 and 2 GGy) samples. Vickers indentation conducted in atmosphere conditions at 50 g during 15 sec.

be constant during an experiment). In eq.3,  $R$  is the gas constant, and  $T$  is the experimental temperature. Crack propagation in pure silica occurs by hydration (penetration of a water molecule into the glass network) and hydrolysis (breaking of  $\text{Si} - \text{O} - \text{Si}$  network bonds) (Ciccotti (2009)).

Figure 4 left depicts the  $v=f(K_I)$  curves for pristine and irradiated silica glass samples. Results in literature (Wiederhorn (1967); Wiederhorn and Bolz (1970); Prades et al. (2005)) do not evidence a static fatigue limit for pure silica. Within the error bars, results herein do not evidence a static fatigue limit for pristine nor irradiated samples. A small shift in the position, i.e.  $v$  vs  $K_I$ , of the curve is observed. Conversely, no significant variation of the slope is observed between pristine, 1 and 2 GGy samples. Hence, due to experimental uncertainties the authors cannot eliminate the hypothesis that the curves are the same.

Figure 4 right presents variations in the hardness value with irradiation doses. There is a slight tendency for the hardness to decrease at 2 GGy. However, due to the large error bars and limited number of irradiations, the significance of the tendency is inconclusive.

Figure 5 shows a slight difference in the behavior of the glass under high pressure before and after irradiation. Looking at the penetration depth of the Vicker's indenter at 50 g, the indenter penetrates deeper in the pristine sample than the 1 and 2 GGy. Corning 7980<sup>®</sup> samples do not evidence pile up.

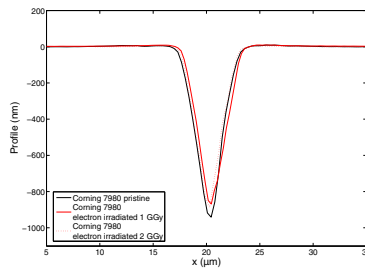


Fig. 5. AFM profiles of indentation on pristine (black line) and irradiated samples 1 (red line) 2 GGy (dotted red line). The maximum indentation load is 50 g, and the profiles are parallel to the edges of indentation. These profiles are the mean of 5 profiles extracted from 5 indentations

#### 4. Discussion

Microscale paramagnetic point defects, revealed by EPR measurements (figure 2), do not scale up to significant variations in the RAMAN spectra (figure 3). This is coherent with literature as  $\text{Si} - \text{O} - \text{Si}$  angle and ring size variations occur in samples subjected to more than 5 GGy electron irradiation (Boizot et al. (2003)). Indeed, defects accumulated in pure silica during irradiation lead at a critical point to slight structural variations.

Figure 4 reveals a small shift in the  $v$  vs  $(f(K_I))$  curves to smaller values for 1 GGy and to larger values for 2 GGy as compared to pristine samples. Several factors can play an important role in this: (1) the small size of the samples requires small loads to propagate crack. Estimated 5% error bar exists on the applied load; (2) samples are not annealed thus residual stresses due to irradiation are possible; and (3) small changes in the experimental offset can appear from one experiment to another. To conclusively elucidate whether or not these shifts are significant, more samples need to be broken at the same doses along with other doses. In the 1970's, Wiederhorn et. al. (Wiederhorn (1967); Wiederhorn and Bolz (1970)) proposed a model (eq. 3) to predict the velocity of the crack front during stress corrosion cracking (in region I). Pure silica has a strong susceptibility to SCC. For the forces applied herein, the stress corrosion crack always propagates. A fatigue limit,  $K_0$  is not expected in pure silica; thus, Maugis and Charles approach ( $K \gg K_0$ ) is applicable (Maugis (1985); Charles (1958)):

$$v^I = v_0 \left( \frac{K}{K_0} \right)^n \quad (4)$$

Table 1 presents  $n$  for pristine, 1 GGy, and 2 GGy irradiated glass samples.

Table 1.  $n$  values determined by power law fit of stress-corrosion curves obtained and  $H_V$  values determined by Vickers indentation for pristine and irradiated pure silica samples.

	Corning 7980 pristine	Corning 7980 1 GGy	Corning 7980 2 GGy
$n$ ( $\text{m}^{3/2}/(\text{MPa}\cdot\text{s}^{-1})$ )	$50_{\pm 10}$	$55_{\pm 5}$	$54_{\pm 15}$
$H_V$ (MPa)	$7820_{\pm 150}$	$7850_{\pm 90}$	$7585_{\pm 100}$

The slopes of the  $v$  vs  $K_I$  curves are steeper for the irradiated samples than pristine samples. Yet due to the uncertainty in the measurements, a conclusive dependence of the slopes on irradiation is not uncovered. Thus to conclusively reveal if  $\beta$ -irradiation alters SCC properties of pure silica more glasses need to be broken. Hardness results unveil similar conclusions.

In general, glasses under high pressure undergo shear flow (Marsh (1964)) (i.e. normal glasses). However,  $\text{SiO}_2$  is the classic example of network former. Pure silica glasses have a tendency to densify under indenter (frequently referred to as "anomalous" glasses in literature (Burghard et al. (2004))). Neely and Mackenzie argued in favor of a deformation by densification as early as 1968 (Neely and Mackenzie (1968)). Recently, Perriot et. al. (Perriot et al. (2006)) evidenced indenter-induced densification via Raman spectra. This study reveals a significant increase in the D1 and D2 bands along with a decrease in the broad peak at  $440 \text{ cm}^{-1}$ . Thus under indenter induced densification the glass forms smaller rings (Perriot et al. (2006)). This scenario is likely herein (under the indenter) as the structure of glass is rather open and the links between tetrahedrons are flexible.

Annealing samples relieves the densification: annealing hydrostatic densified silica at  $1000 \text{ }^\circ\text{C}$  for 1 h permits a volume recovery of more than 99% (Mackenzie (1963a)). Recovery volumes for pristine and irradiated glasses after annealing have been investigated (Table 2).

Figure 6 depicts the variations in the profiles before (solid line) and after annealing (dotted line) for pristine (black) and 2 GGy irradiated samples (red). Similar discrepancies for residual penetration depth occur after annealing. The residual penetration depth after annealing of irradiated glasses is shallower than its pristine counterpart.

Table 2. Recovery volume after annealing for silica glasses non-irradiated and irradiated at 1 and 2 GGy

	Corning 7980 pristine	Corning 7980 1 GGy	Corning 7980 2 GGy
Recovery volume ( $V_R$ )	$89_{\pm 2\%}$	$81_{\pm 2\%}$	$82_{\pm 2\%}$

Table 2 highlights the importance of the densification processes. Permanent deformation under high pressure as expected in literature (Mackenzie (1963a); Yoshida et al. (2005)). For example, Yoshida et al. (2005) evidenced a  $92 \pm 4 \%$  recovery volume (equation 2) for indentation induced densification in silica (annealing temperature was  $0.9T_g$ ). Results herein for pristine samples are in good agreement with results in literature.

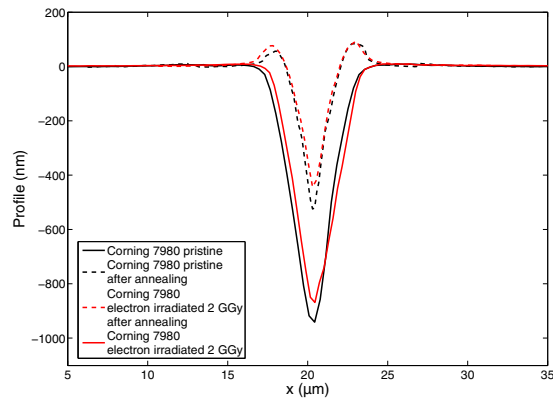


Fig. 6. AFM profiles of indentation on pristine (black line) and irradiated samples at 2 GGy (red line) before (solid line) and after annealing (dotted line) The indentation load is 50 g, and the profiles are parallel to the edges of indentation. These profiles are the mean profiles of 5 profiles extracted from 5 indentations

Buscarino et al. reported local densification in pure amorphous silica ( $\alpha\text{-SiO}_2$ ) depending on electron irradiation doses (Buscarino et al. (2009)). Raman spectra (figure 3) did not reveal any significant variation in the Si – O – Si angle distribution and no clear evidence of densification can be made. This discrepancy can be due to the high OH content in the Corning 7980<sup>®</sup> glasses (800-1000 pm) which can moderate the effect of electron irradiation (Buscarino et al. (2010)). Even if the global structure of silica glasses is not impacted by irradiation, a slight variation in the densification process under high pressure exists. Defects created and stresses induced can make plasticity easier and decrease the densification amount.

## 5. Conclusion

Electron irradiation (0-2 GGy) does induce paramagnetic defects in Corning 7980<sup>®</sup> pure silica samples as evidenced by EPR spectra. This does not lead to significant changes in the structural properties as measured by Raman spectroscopy. Mechanical properties (stress corrosion crack and hardness) are slightly altered due to  $\beta$ -irradiation, but a null response can not be eliminated. More samples at the same and intermediate doses are needed to reduce experimental uncertainties. Higher doses, near 5 GGy, also need to be studied to complete the structural variation and mechanical properties variations analysis.

## 6. Acknowledgements

The authors are grateful to T. Bernard for the technical assistance. Electron irradiations were done at LSI (Laboratoire des Solides Irradiés), Palaiseau, France and supported by the French Network EMIR. This research work is also supported by CEA AREVA, Triangle de la Physique and Ile-de-France (C’Nano and ISC-PIF).

## References

- Agnello, S., Gelardi, F. M., Boscaino, R., Cannas, M., Boizot, B., Petite, G., May 2002. Intrinsic defects induced by beta-irradiation in silica. Nuclear Instruments & Methods In Physics Research Section B-beam Interactions With Materials and Atoms 191, PII S0168–583X(02)00546–3.
- Arora, A., Marshall, D., Lawn, B., 1979. Indentation deformation/fracture of normal and anomalous glasses. Journal of Non-Crystalline Solids 31, 415–428.
- Boizot, B., Agnello, S., Reynard, B., Boscaino, R., Petite, G., Sep. 2003. Raman spectroscopy study of beta-irradiated silica glass. Journal of Non-Crystalline Solids 325 (1-3), 22–28.
- Bonamy, D., Prades, S., Rountree, C. L., Ponson, L., Dalmas, D., Bouchaud, E., Ravi-Chandar, K., Guillot, C., JUL 2006. Nanoscale damage during fracture in silica glass. International Journal of Fracture 140 (1-4), 3–14.

- Bridgman, P. W., Simon, I., 1953. Effect of very high pressure on glass. *Journal of Applied Physics* 24, 405–413.
- Burghard, Z., Zimmermann, A., Rodel, J., Aldinger, F., Lawn, B., 2004. Crack opening profiles of indentation cracks in normal and anomalous glasses. *Acta Materialia* 52, 293–297.
- Buscarino, G., Agnello, S., Gelardi, F. M., 2009. Structural modifications induced by electron irradiation in  $\text{SiO}_2$  glass: Local densification measurements. *Europhysics Letters* 87, 26007 1–4.
- Buscarino, G., Agnello, S., Gelardi, F. M., Boscaino, R., 2010. The role of impurities in the irradiation induced densification of amorphous  $\text{SiO}_2$ . *Journal of Physics Condensed Matter* 22, 255403 1–7.
- Celarie, F., Ciccotti, M., Marliere, C., 2007. Stress-enhanced ion diffusion at the vicinity of a crack tip as evidenced by atomic force microscopy in silicate glasses. *Journal of Non-Crystalline Solids* 353, 51–68.
- Celarie, F., Prades, S., Bonamy, D., Ferrero, L., Bouchaud, E., Guillot, C., Marliere, C., 2003. Glass breaks like metal, but at the nanometer scale. *Physical Review Letters* 90, 1–4.
- Charles, R. J., 1958. Static fatigue of glass. *Journal of Applied Physics* 29, 1549–1662.
- Ciccotti, M., 2009. Stress-corrosion mechanisms in silicate glasses. *Journal of Physics D-applied Physics* 42, 214006 1–18.
- Ernsberg, F., 1968. Role of densification in deformation of glasses under point loading. *Journal of the American Ceramic Society* 51, 545–547.
- Griscom, D., 2011. Trapped-electron centers in pure and doped glassy silica : A review and synthesis. *Journal of Non-Crystalline Solids* 357, 1945–1962.
- He, M., Turner, M. G., E. A., 1995. Analysis of the double cleavage drilled compression specimen for interface fracture energy measurements over a range of mode mixities. *Acta Metallurgica et Materialia* 43, 3453–3458.
- Hetherington, G., 1964. The viscosity of vitreous silica. *Physics and Chemistry of Glasses* 5, 130–136.
- Janssen, C., 1974. Specimen for fracture mechanics studies on glass, ceramic society of japan. *Proceedings 10th International Congress on Glass*, 10.23–10.30.
- Kalia, R. K., Nakano, A., Vashishta, P., Rountree, C. L., Brutzel, L. V., Ogata, S., MAY 2003. Multiresolution atomistic simulations of dynamic fracture in nanostructured ceramics and glasses. *International Journal of Fracture* 121 (1-2), 71–79.
- Lechenault, F., Pallares, G., George, M., Rountree, C., Bouchaud, E., Ciccotti, M., 2010. Effects of finite probe size on self-affine roughness measurements. *Physical Review Letters* 104, 025502 1–4.
- Lechenault, F., Rountree, C., Cousin, F., Bouchaud, J., Ponson, L., Bouchaud, E., 2011. Damage of silicate glasses during stress corrosion. *Journal of Physics Conference Series* 319, 1–11.
- Mackenzie, J., 1963a. High-pressure effects on oxide glasses. 1. densification in rigid state. *Journal of the American Ceramic Society* 46, 461–470.
- Mackenzie, J., 1963b. High-pressure effects on oxide glasses. 2. subsequent heat treatment. *Journal of the American Ceramic Society* 46, 470–476.
- Marsh, D., 1964. Plastic flow in glass. *Proceedings of the Royal Society of London* 282, 33–43.
- Maugis, D., 1985. Review : Subcritical crack growth, surface energy, fracture toughness, stick-slip and embrittlement. *Journal of Materials Science* 20, 3041–3073.
- Neely, J., Mackenzie, J., 1968. Hardness and low-temperature deformation of silica glass. *Journal of Material Science* 3, 603–609.
- Pallares, G., Ponson, L., Grimaldi, A., George, M., Prevot, G., Ciccotti, M., Mar. 2009. Crack opening profile in dcdc specimen. *International Journal of Fracture* 156 (1), 11–20.
- Perriot, A., Barthel, E., Kermouche, G., Querel, G., Vandembroucq, D., 2011. On the plastic deformation of soda-lime glass - a  $\text{Cr}^{3+}$  luminescence study of densification. *Philosophical Magazine* 91, 1245–1255.
- Perriot, A., Vandembroucq, D., Barthel, E., Martinez, V., Grosvalet, L., Martinet, C., Champagnon, B., 2006. Raman microspectroscopic characterization of amorphous silica plastic behavior. *Journal of the American Ceramic Society* 89, 596–601.
- Prades, S., Bonamy, D., Dalmas, D., Bouchaud, E., Guillot, C., 2005. Nano-ductile crack propagation in glasses under stress corrosion: spatiotemporal evolution of damage in the vicinity of the crack tip. *International Journal of Solids and Structures* 42, 637–645.
- Rountree, C., Bonamy, D., Dalmas, D., Prades, S., Kalia, R., Guillot, C., Bouchaud, E., 2010. Fracture in glass via molecular dynamics simulations and atomic force microscopy experiments. *Physics and Chemistry of Glasses-B* 51, 127–132.
- Rountree, C., Kalia, R., Lidorikis, E., Nakano, A., Brutzel, V., Vashishta, P., 2002. Atomistic aspects of crack propagation in brittle materials: Multimillion atom molecular dynamics simulations. *Annual review of Materials Research* 32, 377–400.
- Rountree, C., Prades, S., Bonamy, D., Bouchaud, E., Kalia, R., Guillot, C., 2007. A unified study of crack propagation in amorphous silica: Using experiments and simulations. *Journal of Alloys and Compounds* 434, 60–63.
- Weeks, R., 1956. Paramagnetic resonance of lattice defects in irradiated quartz. *Journal of Applied Physics* 27, 1376–1381.
- Wiederhorn, S., 1967. Influence of water vapor on crack propagation in soda-lime glass. *American Ceramic Society Bulletin* 50, 407–414.
- Wiederhorn, S., Bolz, L., 1970. Stress corrosion and static fatigue of glass. *Journal of the American Ceramic Society* 53, 543–548.
- Wiederhorn, S. M., Guin, J.-P., Fett, T., 2007a. The use of atomic force microscopy to study crack tips in glass. *Geochimica et Cosmochimica Acta* 71, A1110.
- Wiederhorn, S. M., Lopez-Cepero, J. M., Wallace, J., Guin, J.-P., Fett, T., 2007b. Roughness of glass surfaces formed by sub-critical crack growth. *Journal of the Non-Crystalline Solids* 353, 1582–1591.
- Yoshida, S., Isono, S., Matsuoka, J., Soga, N., 2001. Shrinkage behavior of knoop indentations in silica and sodalimesilica glasses. *Journal of the American Ceramic Society* 84, 2141–2143.
- Yoshida, S., Sangleboeuf, J.-C., Rouxel, T., 2005. Quantitative evaluation of indentation-induced densification in glass. *Journal of Material Research* 20, 3404–3412.
- Yoshida, S., Sangleboeuf, J.-C., Rouxel, T., 2007. Indentation-induced densification of soda-lime silicate glass. *International Journal of Materials Research* 98, 360–364.